Production and polarization of prompt $\Upsilon(n\mathrm{S})$ in the improved color evaporation model using the k_T-factorization approach

Vincent Cheung
Department of Physics, University of California, Davis, Davis, California 95616, USA

Ramona Vogt
Nuclear and Chemical Sciences Division, Lawrence Livermore National Laboratory, Livermore, California 94551, USA
and Department of Physics, University of California, Davis, Davis, California 95616, USA

(Received 26 November 2018; published 15 February 2019)

We calculate the polarization of prompt $\Upsilon(n\mathrm{S})$ production in the improved color evaporation model at leading order employing the k_T-factorization approach. We present the polarization parameter λ_ϑ of prompt $\Upsilon(n\mathrm{S})$ as a function of transverse momentum in $p+p$ and $p+\bar{p}$ collisions to compare with data in the helicity, Collins-Soper and Gottfried-Jackson frames. We also present calculations of the bottomonium production cross sections as a function of transverse momentum and rapidity. This is the first p_T-dependent calculation of bottomonium production and polarization in the improved color evaporation model. We find agreement with both bottomonium cross sections and polarization measurements.

DOI: 10.1103/PhysRevD.99.034007

I. INTRODUCTION

This paper is a continuation of our previous work [1] on quarkonium production and polarization in the improved color evaporation model using the k_T-factorization approach.

We first developed our LO calculation of quarkonium polarization in the ICEM [2] in Refs. [3,4] employing collinear factorization. However, in this framework, we were unable to address the polarization as a function of p_T to compare with collider data. Therefore, we performed the first p_T-dependent polarization calculation in the ICEM [1] for prompt J/ψ production and polarization by employing the k_T-factorization approach. This paper is a continuation of that work where we now extend our p_T-dependent leading order (LO) ICEM calculation of quarkonium production and polarization in the k_T-factorization approach to prompt $\Upsilon(n\mathrm{S})$. We use the same scattering amplitudes as in Ref. [1]. This work also provides the first p_T-dependent ICEM $\Upsilon(n\mathrm{S})$ polarization result. We will begin to address the p_T dependence at NLO in a later publication.

We note that within the framework of nonrelativistic QCD (NRQCD) [5], the quarkonium polarization problem is less prominent in bottomonium than in charmonium. Fitting the long distance matrix elements to measurements of Υ yields and polarization for $p_T > 8$ GeV, NRQCD is able to provide a better description of bottomonium yields and polarization than for charmonium [6,7]. The heavier bottom quark mass allows better convergence of the double expansion in α_s and v. Reference [8] derived a relationship between the traditional CEM and NRQCD assuming that NRQCD factorization holds to all orders and that the NRQCD sums over color and spin converge. It also assumed that no distinction is made between the spin states in the CEM.

II. PRODUCTION OF POLARIZED BOTTOMONIUM IN THE k_T-FACTORIZATION APPROACH

In this paper, we present both the yields and polarizations of bottomonium as a function of p_T by formulating the ICEM in the k_T-factorization approach. We take the same effective Feynman rules for scattering processes involving incoming off-shell gluons [9] as in the NRQCD calculation of Ref. [10]. Effectively, the momentum of the incoming Reggeon, k^μ, with transverse momentum k_T can be written in terms of the proton momentum p^μ and the fraction of longitudinal momentum x carried by the gluon as

$$k^\mu = xp^\mu + k_T^\mu. \tag{1}$$

The polarization 4-vector is

$$\epsilon^\mu(k_T) = \frac{k_T^\mu}{k_T}, \tag{2}$$

where $k_T^\mu = (0, \vec{k}_T, 0)$.

In the traditional CEM, all bottomonium states are treated the same as $b\bar{b}$ below the $B\bar{B}$ threshold. The invariant mass of the heavy $b\bar{b}$ pair is restricted to be less than twice the mass of the lowest mass B meson. The distributions for all bottomonium family members are assumed to be identical. In the ICEM, the invariant mass of the intermediate $b\bar{b}$ pair is constrained to be larger than the mass of produced bottomonium state, $M_{\mathcal{Q}}$, instead of twice the bottom quark mass, $2m_b$, the lower limit in the traditional CEM [4,11]. Because the bottomonium momentum and integration range now depend on the mass of the state, the kinematic distributions of the bottomonium states are no longer identical in the ICEM. Using the k_T-factorization approach, in a $p+p$ collision the ICEM production cross section for a directly-produced bottomonium state $\mathcal{Q}$ is

$$\begin{aligned}\sigma = F_{\mathcal{Q}} \int_{M_{\mathcal{Q}}^2}^{4m_B^2} d\hat{s} \int \frac{dx_1}{x_1} \int \frac{d\phi_1}{2\pi} \int d{k_{1T}}^2 \Phi_1(x_1, k_{1T}, \mu_{F1}^2) \\ \times \int \frac{dx_2}{x_2} \int \frac{d\phi_2}{2\pi} \int d{k_{2T}}^2 \Phi_2(x_2, k_{2T}, \mu_{F2}^2) \hat{\sigma}(R+R \to Q\bar{Q}) \\ \times \delta(\hat{s} - x_1 x_2 s + |\vec{k}_{1T} + \vec{k}_{2T}|^2), \end{aligned} \tag{3}$$

where the square of the heavy quark pair invariant mass is $\hat{s}$ while the square of the center-of-mass energy in the $p+p$ collision is s. Here $\Phi(x, k_T, \mu_F^2)$ is the unintegrated parton distribution function (uPDF) for a Reggeized gluon with a momentum fraction x and a transverse momentum k_T interacting with a factorization scale μ_F. The angles $\phi_{1,2}$ in Eq. (3) are between the $k_{T1,2}$ of the partons and the p_T of the final state bottomonium $\mathcal{Q}$. The parton-level cross section is $\sigma(R+R \to b\bar{b})$. Finally, $F_{\mathcal{Q}}$ is a universal factor for the directly-produced bottomonium state $\mathcal{Q}$, and is independent of the projectile, target, and energy. In this approach, the cross section is

$$\begin{aligned}\frac{d^4\sigma}{dp_T dy d\hat{s} d\phi} &= \sigma \delta(\hat{s} - x_1 x_2 s + p_T^2) \delta\left(y - \frac{1}{2}\log\frac{x_1}{x_2}\right) \\ &\quad \times \delta(p_T^2 - |\vec{k}_{1T}^2 + \vec{k}_{2T}^2|) \delta(\phi - (\phi_1 - \phi_2)) \\ &= F_{\mathcal{Q}} \int \frac{2}{\pi} k_{2T} dk_{2T} \sum_{k_{1T}} \left[\frac{\Phi_1(k_{1T}, x_{10}, \mu_{F1}^2)}{x_{10}} \right. \\ &\quad \times \frac{\Phi_2(k_{2T}, x_{20}, \mu_{F2}^2)}{x_{20}} k_{1T} p_T \\ &\quad \left. \times \frac{\hat{\sigma}(R+R \to Q\bar{Q})}{s\sqrt{k_{2T}^2(\cos^2\phi - 1) + p_T^2}} \right] \end{aligned} \tag{4}$$

where the sum k_{1T} is over the roots of $k_{1T}^2 + k_{2T}^2 + 2k_{1T}k_{2T}\cos\phi = p_T^2$, and $k_{1T,1}$, $k_{1T,2}$ are

$$k_{1T,1} = -k_{2T}\cos\phi + \sqrt{k_{2T}^2(\cos^2\phi - 1) + p_T^2} \tag{5}$$

$$k_{1T,2} = -k_{2T}\cos\phi - \sqrt{k_{2T}^2(\cos^2\phi - 1) + p_T^2}. \tag{6}$$

The momentum fractions x_{10} and x_{20} are

$$x_{10} = \sqrt{\frac{\hat{s} + p_T^2}{s}} e^{+y}, \tag{7}$$

$$x_{20} = \sqrt{\frac{\hat{s} + p_T^2}{s}} e^{-y}. \tag{8}$$

Here, ϕ is the relative azimuthal angle between two incident Reggeons ($\phi = \phi_1 - \phi_2$) and p_T is the transverse momentum of the produced $b\bar{b}$.

Thus the transverse momentum distribution $d\sigma/dp_T$ in the ICEM is

$$\frac{d\sigma}{dp_T} = \int dy d\hat{s} d\phi \frac{d^4\sigma}{dp_T dy d\hat{s} d\phi}. \tag{9}$$

We integrate over rapidity to compare to collider data with defined rapidity cuts. Similarly, the rapidity distribution $d\sigma/dy$ in the ICEM is

$$\frac{d\sigma}{dy} = \int dp_T d\hat{s} d\phi \frac{d^4\sigma}{dp_T dy d\hat{s} d\phi}. \tag{10}$$

As our central result, we take the renormalization and factorization scales to be $\mu_F = \mu_R = m_T$, where m_T is the transverse mass of the $b\bar{b}$. We will study the effect of varying these scales on the p_T distributions and the polarization.

III. POLARIZATION OF PROMPT $\Upsilon(nS)$

We employ the scattering amplitudes calculated in Ref. [1] to compute the $b\bar{b}$ partonic production cross section $\hat{\sigma}^{J,J_z}$ according to the J^P of each directly produced bottomonium state below the $B\bar{B}$ threshold. We then convolute the polarized partonic cross sections with the uPDFs to obtain the hadron-level cross section, σ, as a function of p_T using Eq. (9). The bottomonium masses which appear as the lower limit of the $b\bar{b}$ invariant mass in the calculations of $\hat{\sigma}^{J,J_z}$ are listed in Table I. We employ the ccfm-JH-2013-set1 [12] uPDFs in this calculation.

We assume that the angular momentum of each directly-produced bottomonium state is unchanged by the transition from the parton level to the hadron level, consistent with the CEM expectation that the linear momentum is unchanged by hadronization.

We calculate the ratio of the individual $J_z = 0, \pm 1$ to the unpolarized partonic cross sections ratios for each directly-produced bottomonium state $\mathcal{Q}$ that has a contribution to prompt $\Upsilon(n\mathrm{S})$ production: $\Upsilon(1\mathrm{S})$, $\Upsilon(2\mathrm{S})$, $\Upsilon(3\mathrm{S})$, $\chi_{b1}(1\mathrm{P})$,

TABLE I. The mass, $M_{\mathcal{Q}}$, and the squared feed-down transition Clebsch-Gordan coefficients, $S_{\mathcal{Q}}^{J_z}$, for all bottomonium states contributing to prompt $\Upsilon(n\mathrm{S})$ production.

$\mathcal{Q}$	$M_{\mathcal{Q}}$ (GeV)	$S_{\mathcal{Q}}^{J_z=0}$	$S_{\mathcal{Q}}^{J_z=\pm1}$
$\Upsilon(1\mathrm{S})$	9.46	1	0
$\Upsilon(2\mathrm{S})$	10.02	1	0
$\Upsilon(3\mathrm{S})$	10.36	1	0
$\chi_{b1}(1\mathrm{P})$	9.89	0	1/2
$\chi_{b2}(1\mathrm{P})$	9.91	2/3	1/2
$\chi_{b1}(2\mathrm{P})$	10.26	0	1/2
$\chi_{b2}(2\mathrm{P})$	10.27	2/3	1/2
$\chi_{b1}(3\mathrm{P})$	10.51	0	1/2
$\chi_{b2}(3\mathrm{P})$	10.51	2/3	1/2

$\chi_{b2}(1\mathrm{P})$, $\chi_{b1}(2\mathrm{P})$, $\chi_{b2}(3\mathrm{P})$, $\chi_{b1}(3\mathrm{P})$, and $\chi_{b2}(3\mathrm{P})$. These ratios, $R_{\mathcal{Q}}^{J_z}$, are then independent of $F_{\mathcal{Q}}$. We assume the feed-down production of $\Upsilon(n\mathrm{S})$ from the higher mass bound states follows the angular momentum algebra. Their contributions of these higher states to $R_{\Upsilon(n\mathrm{S})}^{J_z=0}$ for prompt $\Upsilon(n\mathrm{S})$ are added after weighting by the feed-down contribution ratios $c_{\mathcal{Q}}$ [13]:

$$R_{\Upsilon}^{J_z=0} = \sum_{\mathcal{Q},J_z} c_{\mathcal{Q}} S_{\mathcal{Q}}^{J_z} R_{\mathcal{Q}}^{J_z}. \tag{11}$$

Here $S_{\mathcal{Q}}^{J_z}$ is the transition probability from a given state $\mathcal{Q}$ produced in a J_z state to a $\Upsilon(n\mathrm{S})$ with $J_z = 0$ in a single decay. We assume two pions are emitted for S state feed down, $\Upsilon(2\mathrm{S}) \to \Upsilon(1\mathrm{S})\pi\pi$, and a photon is emitted for a P state feed down, $\chi_b(1\mathrm{P}) \to \Upsilon(1\mathrm{S})\gamma$. $S_{\mathcal{Q}}^{J_z}$ is then 1 (if $J_z = 0$) or 0 (if $J_z = 1$) for $\mathcal{Q} = \Upsilon(2\mathrm{S})$ since the transition, $\Upsilon(2\mathrm{S}) \to \Upsilon(1\mathrm{S})\pi\pi$, does not change the angular momentum of the quarkonium state. For directly produced $\Upsilon(n\mathrm{S})$, $S_{\mathcal{Q}}^{J_z}$ is 1 for $J_z = 0$ and 0 for $J_z = 1$. The $S_{\mathcal{Q}}^{J_z}$ for the χ states are the squares of the Clebsch-Gordan coefficients for the feed-down production via $\chi_b \to \Upsilon(n\mathrm{S})\gamma$. The bottomonium feed-down ratios are p_T-dependent [13]: the fraction of direct production is larger at low p_T than at high p_T. We consider two sets of feed-down ratios from Ref. [13]. These ratios are derived from LHC measurements [14–22] assuming they vary with p_T but not rapidity [13]. The "low p_T" ratios are used to compare with LHCb data ($0 < p_T < 20$ GeV) where the "high p_T" ratios are employed to compare with CMS data ($10 < p_T < 50$ GeV). Here, we are assuming the feed-down contribution from $\chi_{b1}(n\mathrm{P})$ and $\chi_{b2}(n\mathrm{P})$ are the same as in our previous approach for the χ_c states [3]. A similar assumption is made for the other P states. The values of $M_{\mathcal{Q}}$ and $S_{\mathcal{Q}}^{J_z}$ for all bottomonium states contributing to prompt $\Upsilon(n\mathrm{S})$ production are collected in Table I and the values of $c_{\mathcal{Q}}$ in the two p_T regions are presented in Table II.

Finally, the $J_z = 0$ to the unpolarized ratio for prompt $\Upsilon(n\mathrm{S})$ states are converted into the polarization parameter λ_ϑ [23],

$$\lambda_\vartheta = \frac{1 - 3R^{J_z=0}}{1 + R^{J_z=0}}, \tag{12}$$

where $-1 < \lambda_\vartheta < 1$. If $\lambda_\vartheta = -1$, $\Upsilon(n\mathrm{S})$ production is totally longitudinal, $\lambda_\vartheta = 0$ refers to unpolarized production, while production is totally transverse for $\lambda_\vartheta = +1$.

IV. RESULTS

Although the matrix elements in this calculation are LO in α_s, by convoluting the polarized partonic cross sections with the transverse momentum dependent uPDFs using the k_T-factorization approach, we can calculate the yield as well as the polarization parameter λ_ϑ as a function of p_T. The full NLO polarization, including $q\bar{q}$ and $(q + \bar{q})g$ contributions, will be discussed in a future publication.

The traditional CEM can describe the unpolarized yields of $\Upsilon(n\mathrm{S})$ production at NLO assuming collinear factorization [24]. In this calculation, we take advantage of the

TABLE II. The feed-down ratios, $c_{\mathcal{Q}}$, for prompt $\Upsilon(1\mathrm{S})$, $\Upsilon(2\mathrm{S})$, and $\Upsilon(3\mathrm{S})$ production from direct $\Upsilon(1\mathrm{S})$, $\Upsilon(2\mathrm{S})$, $\Upsilon(3\mathrm{S})$, $\chi_b(1P)$, $\chi_b(2P)$, and $\chi_b(3P)$ in the low p_T and high p_T regions [13]. We assume the feed-down contributions from $\chi_{b1}(n\mathrm{P})$ and $\chi_{b2}(n\mathrm{P})$ are the same as also done in Ref. [3].

	Low p_T $c_{\mathcal{Q}}$ ($p_T \lesssim 20$ GeV)			High p_T $c_{\mathcal{Q}}$ ($p_T \gtrsim 20$ GeV)		
$\mathcal{Q}$ (direct\prompt)	$\Upsilon(1\mathrm{S})$	$\Upsilon(2\mathrm{S})$	$\Upsilon(3\mathrm{S})$	$\Upsilon(1\mathrm{S})$	$\Upsilon(2\mathrm{S})$	$\Upsilon(3\mathrm{S})$
$\Upsilon(1\mathrm{S})$	0.71	...	...	0.45	...	...
$\Upsilon(2\mathrm{S})$	0.07	0.73	...	0.14	0.60	...
$\Upsilon(3\mathrm{S})$	0.01	0.04	0.70	0.03	0.05	0.50
$\chi_{b1}(1\mathrm{P})$	0.075	...	...	0.145	...	...
$\chi_{b2}(1\mathrm{P})$	0.075	...	...	0.145	...	...
$\chi_{b1}(2\mathrm{P})$	0.02	0.10	...	0.03	0.15	...
$\chi_{b2}(2\mathrm{P})$	0.02	0.10	...	0.03	0.15	...
$\chi_{b1}(3\mathrm{P})$	0.01	0.015	0.15	0.015	0.025	0.25
$\chi_{b2}(3\mathrm{P})$	0.01	0.015	0.15	0.015	0.025	0.25

ICEM to calculate the direct production of the individual bottomonium states separately. Since this is the first bottomonium calculation in the ICEM using the k_T-factorization approach, it is important to check if our calculated unpolarized yields are also in agreement with the data.

We first check how our approach describes the transverse momentum and rapidity distribution of the bottomonium states at collider energies. We then discuss the transverse momentum dependence of the polarization parameter λ_ϑ for prompt $\Upsilon(n\mathrm{S})$ production. We compare our results to the polarization measured in collider experiments in the helicity (HX), Collins-Soper (CS) [25], and Gottfried-Jackson (GJ) [26] frames to discuss the frame dependence of λ_ϑ. W also discuss the sensitivity of our results to the bottom quark mass, the renormalization scale, and the feed-down ratios. In our calculations, we construct the uncertainty bands by varying the bottom quark mass around its base value of 4.75 GeV, in the interval $4.5 < m_b < 5$ GeV, and the renormalization scale around its base value of m_T, in the interval $0.5 < \mu_R/m_T < 2$, while keeping the factorization scale fixed at $\mu_F = m_T$. The total uncertainty band is constructed by adding the mass and renormalization scale uncertainties in quadrature. We do not extend our calculation below $p + \bar{p}$ at Tevatron energies because at fixed-target energies and even at the RHIC collider the k_T-factorization approach with off-shell gluons is inappropriate for bottomonium.

A. Unpolarized bottomonium production

Here, we present the p_T and rapidity distributions of the $\Upsilon(n\mathrm{S})$ states as well as the ratio of $\chi_{b1}(1\mathrm{P})$ to $\chi_{b2}(1\mathrm{P})$ in our approach. In the spirit of the traditional CEM, $F_{\mathcal{Q}}$ in Eq. (3) has to be independent of the projectile, target, and energy for each bottomonium state $\mathcal{Q}$. Even though the focus of this paper is on polarization, independent of $F_{\mathcal{Q}}$, the unpolarized bottomonium yields in the ICEM using the k_T-factorization approach were not calculated before. Therefore, it is important to first confirm that this approach can indeed describe the bottomonium yields as a function of p_T and rapidity before discussing polarization. The direct production cross section is calculated using Eq. (9) by integrating the pair invariant mass from $M_{\mathcal{Q}}$ to $2m_{B^0}$ ($m_{B^0} = 5.28$ GeV).

We first obtain $F_{\Upsilon(n\mathrm{S})}$ by comparing our results with the $\Upsilon(n\mathrm{S})$ yields measured by the CMS Collaboration at 7 TeV. Using the same $F_{\Upsilon(n\mathrm{S})}$, we compare our results with the $\Upsilon(n\mathrm{S})$ data measured at CDF and LHCb.

1. $\Upsilon(1\mathrm{S})$ p_T distribution

We found in our previous paper [1] that the charmonium p_T distribution has a significant dependence on the factorization scale for $p_T > 5$ GeV. In this paper, we also fix the factorization scale at $\mu_F = m_T$ instead of including a factor of two variation. In Fig. 1, we show the p_T distributions of prompt $\Upsilon(1\mathrm{S})$ production at $\sqrt{s} = 7$ TeV found by fixing $m_b = 4.75$ GeV and varying the factorization scale over the range $0.5 < \mu_F/m_T < 2$ and the renormalization scale over the range $0.5 < \mu_R/m_T < 2$ separately. We also fix $\mu_F/m_T = \mu_R/m_T = 1$ and vary the bottom quark mass over the range $4.5 < m_b < 5$ GeV. The direct production cross section is calculated using Eq. (9) by integrating the pair invariant mass from $M_{\Upsilon(1\mathrm{S})}$ to $2m_{B^0}$ ($m_{D^0} = 5.28$ GeV) over the rapidity range $|y| < 2.4$. We assume that direct production is a constant fraction, 0.71 of the prompt production, according to the low p_T feed-down coefficients in Table II, since the yield is dominated by production at low p_T. We then compare the prompt p_T distribution in the ICEM with the CMS data [22]. Similar to the charmonium p_T distribution, the result has a significant dependence on the factorization scale for $p_T > 5$ GeV. This is because the uPDFs have a sharp cutoff for $k_T > \mu_F$ and are thus very sensitive to the chosen factorization scale. The yield varies more as p_T approaches m_T at high p_T. At low p_T, $m_T \sim M_{\mathcal{Q}}$ and the cross section is independent of the factorization scale since $k_T \ll \mu_F$. At moderate p_T, the variation with μ_F is similar to or smaller than that due to the bottom quark mass. At $p_T \sim 10$ GeV, $m_T \sim p_T$. Thus the lower limit on the factorization scale, $m_T/2$, is on the order of k_T and the yield drops off at this cutoff limit of ~5 GeV, while the upper limit on the factorization scale, $2m_T$, is still greater than k_T, enhancing the yield. Since, at LO, only the $b\bar{b}$ pair carries the transverse momentum, the predictive power for the yields is limited by the uPDFs. Therefore, to construct a meaningful uncertainty band, we fix the factorization scale at $\mu_F = m_T$. As we push toward the limit of the k_T-factorization approach with uPDFs at high p_T at LO, we can only improve the high p_T limit by a full NLO calculation in the collinear factorization approach where there is no hard limit on μ_F as in k_T-factorization approach.

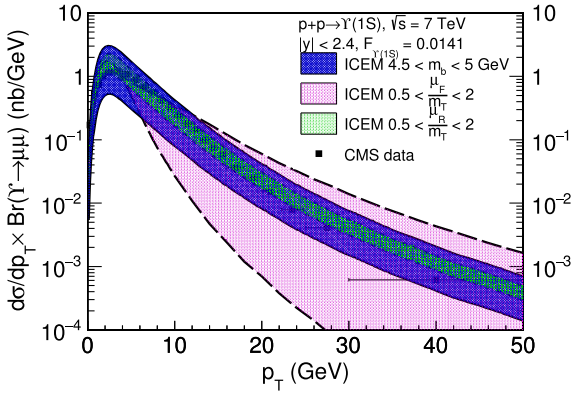

FIG. 1. The p_T dependence of prompt $\Upsilon(1\mathrm{S})$ production at $\sqrt{s} = 7$ TeV in the ICEM obtained by varying the bottom quark mass (blue), the factorization scale in the range $0.5 < \mu_F/m_T < 2$ (magenta), and the renormalization scale in the range $0.5 < \mu_R/m_T < 2$ (green) is compared with the CMS midrapidity data [22].

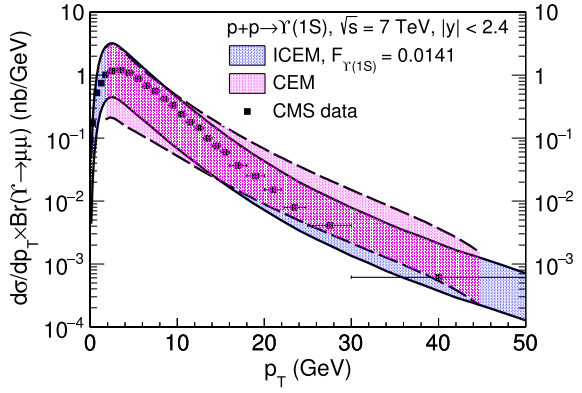

FIG. 2. The p_T dependence of prompt $\Upsilon(1S)$ production at $\sqrt{s} = 7$ TeV in the ICEM with combined mass and renormalization scale uncertainties (blue) and that in the CEM using collinear factorization approach (magenta). The CMS midrapidity data [22] from Fig. 1 are also shown.

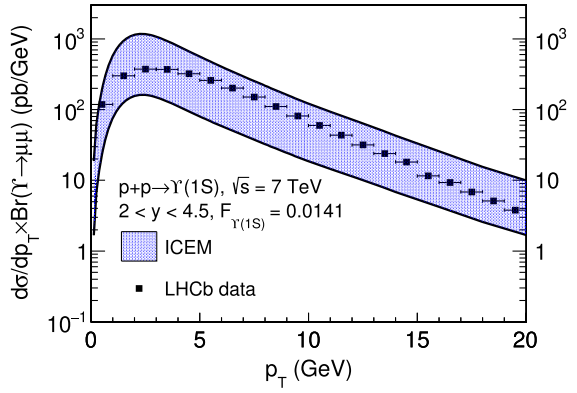

FIG. 3. The p_T dependence of prompt $\Upsilon(1S)$ production at $\sqrt{s} = 7$ TeV and $2 < y < 4.5$ in the ICEM with combined mass and renormalization scale uncertainties is compared with the LHCb data [27].

After fixing the factorization scale, the variation in bottom quark mass then gives the largest uncertainty, followed by the variation in renormalization scale. When μ_R is reduced, the strong coupling constant is larger, increasing the yield. On the other hand, when m_b is reduced, the yield increases. In the remainder of this section, we present our results by adding the uncertainties due to variations of the bottom mass and renormalization scale in quadrature.

The prompt $\Upsilon(1S)$ p_T distribution at $\sqrt{s} = 7$ TeV with combined uncertainty is shown in Fig. 2. The ICEM result has a peak at $p_T \sim 2.5$ GeV, in agreement with the data. By matching to the total experimental unpolarized yield in $|y| < 2.4$, we find that the ICEM can describe the $\Upsilon(1S)$ p_T distribution with $F_{\Upsilon(1S)} = 0.0141$. This is the fraction of $b\bar{b}$ pairs produced in the invariant mass range from $M_{\Upsilon(1S)}$ to $2m_{B^0}$, a difference of ~1 GeV, that result in direct $\Upsilon(1S)$ production, defined in Eq. (3). In general, the ICEM p_T distribution agrees with the data for all p_T.

In the same figure, we compare the inclusive $\Upsilon(1S)$ p_T distributions with that from the CEM in the collinear factorization approach. The uncertainty band is constructed by combining the uncertainty by varying the bottom mass in the range $4.56 < m_b < 4.74$ GeV, the factorization scale in the range $0.91 < \mu_F/m_T < 2.17$, and the renormalization scale in the range $0.9 < \mu_R/m_T < 1.32$. We find two distributions agree reasonably well with each other and the data.

We test the universality of $F_{\Upsilon(1S)}$ by comparing the prompt $\Upsilon(1S)$ p_T distribution in the ICEM measured by LHCb [27] at $\sqrt{s} = 7$ TeV and $2 < y < 4.5$ in Fig. 3 and to the prompt $\Upsilon(1S)$ p_T distribution measured by D0 [28] at $\sqrt{s} = 1.8$ TeV and $|y| < 0.5$ in Fig. 4. We again assume the direct production is a constant fraction, 0.71, of the prompt production to obtain the prompt $\Upsilon(1S)$ cross section. We find the ICEM result agrees with the data for all p_T.

2. $\Upsilon(2S)$ p_T distribution

The prompt $\Upsilon(2S)$ p_T distribution at $\sqrt{s} = 7$ TeV is compared to the CMS measurement [22] over $|y| < 2.4$ in Fig. 5 and the LHCb data [27] in $2 < y < 4.5$ in Fig. 6. Here, the direct production cross section is calculated using Eq. (9) by integrating the pair invariant mass from $M_{\Upsilon(2S)}$ to $2m_{B^0}$ over the rapidity range $|y| < 2.4$. Similar to direct $\Upsilon(1S)$, we assume the direct production of $\Upsilon(2S)$ is a constant fraction, 0.73, of the prompt production. We then compare the p_T-integrated yield of prompt $\Upsilon(2S)$ with the CMS measurement [22]. By matching the p_T-integrated yield, we find $F_{\Upsilon(2S)} = 0.0144$. We note that $F_{\Upsilon(2S)} \gtrsim F_{\Upsilon(1S)}$, primarily because the integrated mass region is much narrower for $\Upsilon(2S)$ than $\Upsilon(1S)$, a difference of ~0.5 GeV in this case. In the traditional CEM, $F_{\Upsilon(2S)}$ is smaller than $F_{\Upsilon(1S)}$ because the range of integration over the pair invariant mass is the same for all $\Upsilon(n\mathrm{S})$. We find agreement with the data within the combined uncertainty

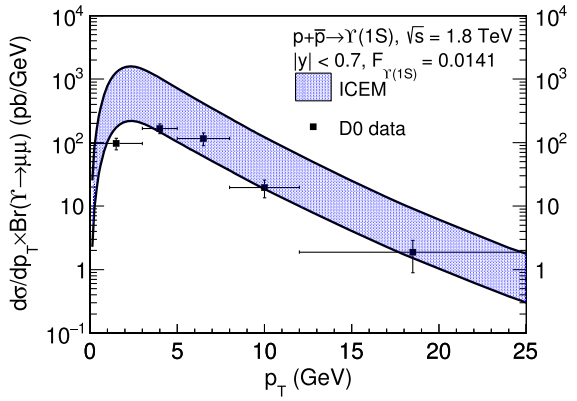

FIG. 4. The p_T dependence of prompt $\Upsilon(1S)$ production at $\sqrt{s} = 7$ TeV and $|y| < 0.7$ in the ICEM with combined mass and renormalization scale uncertainties is compared with the D0 data [28].

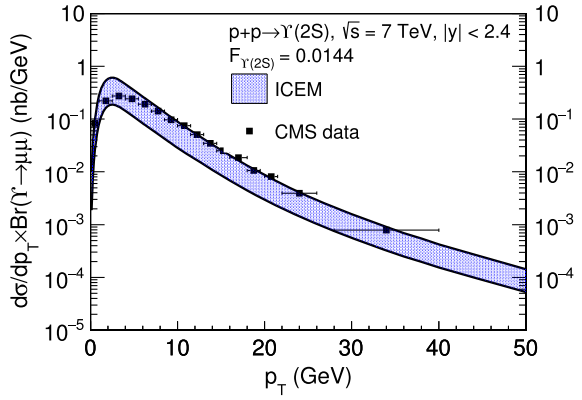

FIG. 5. The p_T dependence of prompt $\Upsilon(2S)$ production at $\sqrt{s} = 7$ TeV and $2 < y < 4.5$ in the ICEM with combined mass and renormalization scale uncertainties is compared with the CMS midrapidity data [22].

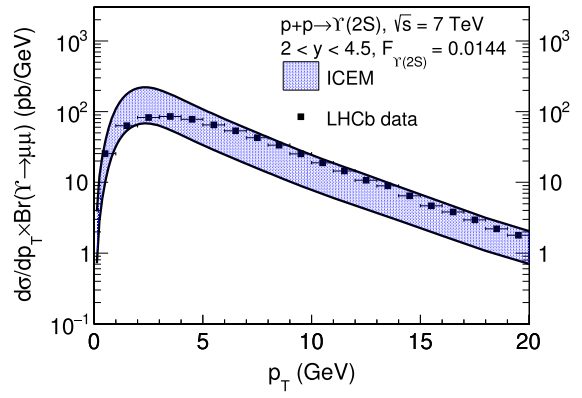

FIG. 6. The p_T dependence of prompt $\Upsilon(2S)$ production at $\sqrt{s} = 7$ TeV and $2 < y < 4.5$ in the ICEM with combined mass and renormalization scale uncertainties is compared with the LHCb data [27].

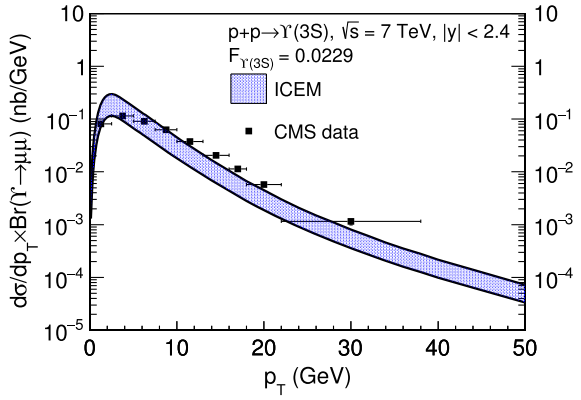

FIG. 7. The p_T dependence of prompt $\Upsilon(3S)$ production at $\sqrt{s} = 7$ TeV in the ICEM with combined mass and renormalization scale uncertainties is compared with the CMS midrapidity data [22].

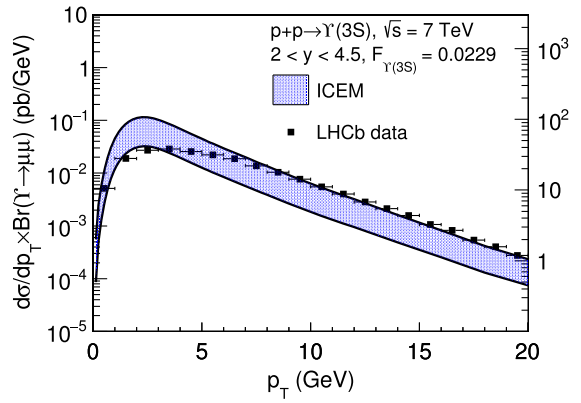

FIG. 8. The p_T dependence of prompt $\Upsilon(2S)$ production at $\sqrt{s} = 7$ TeV and $2 < y < 4.5$ in the ICEM with combined mass and renormalization scale uncertainties is compared with the LHCb data [27].

band constructed by varying the bottom quark mass and the renormalization scale in the ICEM. In both cases, the calculations, with their associated uncertainty bands, are in agreement with the data.

3. $\Upsilon(3S)$ p_T distribution

The prompt $\Upsilon(3S)$ p_T distribution at $\sqrt{s} = 7$ TeV is compared to the CMS measurements [22] over $|y| < 2.4$ in Fig. 7 and the LHCb data [27] in $2 < y < 4.5$ in Fig. 8. Here, the direct production cross section is calculated using Eq. (9) by integrating the pair invariant mass from $M_{\Upsilon(3S)}$ to $2m_{B^0}$ over the rapidity range $|y| < 2.4$. Similar to direct $\Upsilon(1S)$, we assume the direct production of $\Upsilon(3S)$ is a constant fraction, 0.70, of the prompt production. Therefore, we compare the p_T-integrated yield of direct $\Upsilon(3S)$ with the CMS measurement [22]. We find $F_{\Upsilon(3S)} = 0.00229$. We note that also $F_{\Upsilon(3S)} \gtrsim F_{\Upsilon(1S)}$, because the mass range is still smaller for $\Upsilon(3S)$, a difference of only ~0.15 GeV. Again, in the traditional CEM, $F_{\Upsilon(3S)}$ is smaller than $F_{\Upsilon(1S)}$ and $F_{\Upsilon(2S)}$ because the range of integration over the pair invariant mass is also the same for both $\Upsilon(1S)$ and $\Upsilon(3S)$. There is fair agreement with the data within the combined uncertainty band constructed by varying the bottom quark mass and the renormalization scale in the ICEM. In both cases, the calculations, with their associated uncertainty bands, are in agreement with the data.

4. Ratio of $\chi_{b2}(1P)$ to $\chi_{b1}(1P)$ production

We now turn to the p_T dependence of the ratio $\chi_{b2}(1P)/\chi_{b1}(1P)$ as a function of p_T. The ratios of direct $\chi_{b2}(1P)$ to direct $\chi_{b1}(1P)$ at $\sqrt{s} = 8$ TeV at central and forward rapidities are presented in Fig. 9. Direct production is calculated using Eq. (9) by integrating the pair invariant mass from $M_{\chi_{b1,2}}(1P)$ to $2m_{B^0}$ over two rapidity ranges, $|y| < 1.5$ and $2 < y < 4.5$ respectively, in order to compare with existing measurements [29,30]. As there is not enough

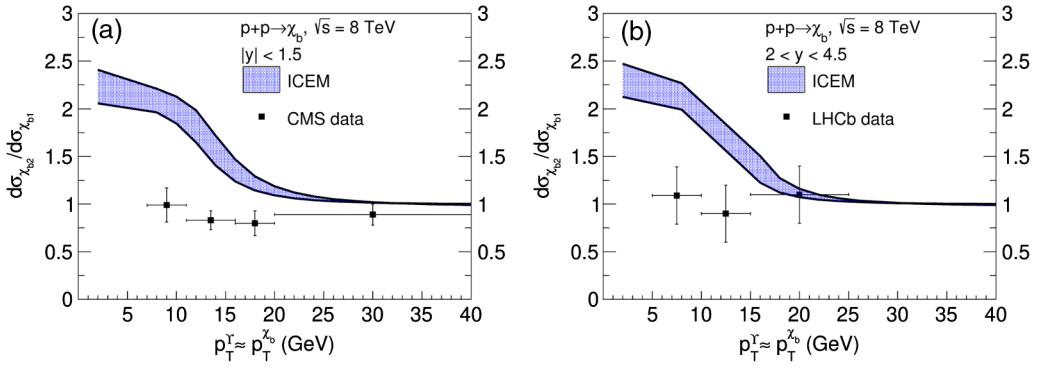

FIG. 9. The ratio of $\chi_{b2}(1P)$ to $\chi_{b1}(1P)$ in the ICEM with combined mass and renormalization scale uncertainties at $\sqrt{s} = 8$ TeV at central rapidity $|y| < 1.5$ (a) and at forward rapidity $2 < y < 4.5$ (b) assuming $F_{\chi_{b1(1P)}} = F_{\chi_{b2(1P)}}$. The CMS data [29] and the LHCb data [30] are also shown in (a) and (b) respectively.

information on the feed-down production to χ_b, we assume the prompt production of $\chi_{b1,2}(1P)$ is approximately the same as the direct production. Since there are no measurements of the absolute $\chi_{b1,2}(1P)$ production cross sections, we cannot fix $F_{\chi_{b1,2}(1P)}$. Furthermore, the data reports the ratio as a function of the p_T of $\Upsilon(1S)$. To compare our results with the data, we then assume that $p_T^{\chi_b} \approx p_T^{\Upsilon(1S)}$, not unreasonable since the mass difference between the states is ~500 MeV and the decay photon is soft. Thus the ICEM can only predict the trend of the relative production subject to an overall vertical shift. Similar to the χ_{c2} to χ_{c1} ratio in the ICEM [1], $\chi_{b2}(1P)/\chi_{b1}(1P)$ becomes constant for $p_T > 2M_{\chi_b}$. However, the relative production decreases with increasing p_T for $p_T < 2M_{\chi_b}$, independent of the rapidity range considered. Our ICEM results only agree with the data in the higher p_T range. This is because the difference between the amplitudes of χ_{b1} and χ_{b2} is most apparent at low p_T since the curvature of the distributions changes fastest near the peaks of the distributions. However, the measured relative production is approximately p_T independent at lower p_T. We note that the χ_{c2}/χ_{c1} ratios presented in Ref. [1] agreed with the data over the measured p_T range because, in that case, $p_T \gg M_{\chi_c}$ over the range of the measurement. However, with the lower p_T range here this condition is not satisfied for χ_b.

5. $\Upsilon(nS)$ rapidity distribution

We now turn to the rapidity dependence of $\Upsilon(nS)$ production. The rapidity distribution of prompt of $\Upsilon(nS)$ at $\sqrt{s} = 7$ TeV is shown in Fig. 10. The direct production is calculated using Eq. (10) by integrating over the p_T range $0 < p_T < 30$ GeV. We again assume the direct production of $\Upsilon(1S, 2S, 3S)$ is a constant 71%, 73%, and 70% of prompt $\Upsilon(1S, 2S, 3S)$ production respectively. We use the same values of $F_{\Upsilon(nS)}$ determined for the p_T distributions to compare the rapidity distribution in the ICEM with the measurement made by the LHCb Collaboration [27]. We find the ICEM can describe the LHCb rapidity distribution at $\sqrt{s} = 7$ TeV using the $F_{\Upsilon(nS)}$ obtained at the same energy by CMS in the central rapidity region.

B. p_T dependence of λ_ϑ

Here, we present the p_T dependence of the polarization parameter λ_ϑ in $p + p$ and $p + \bar{p}$ collisions. Because the polarization parameter is defined as the ratio of polarized to unpolarized cross sections in Eq. (11) and these cross sections depend on μ_R in the same way, the polarization parameter is independent of the scale choice. Note that λ_ϑ is thus also independent of μ_F. However, the amplitudes themselves are mass dependent so that the polarized to unpolarized ratio in λ_ϑ depends on the bottom quark mass. Thus the only uncertainty on λ_ϑ in our calculation is due to the variation of m_b in the range $4.5 < m_b < 5$ GeV. Therefore, in this section, the uncertainty bands only include the mass variation and the uncertainty in the calculated polarization is reduced relative to those of the yield calculations.

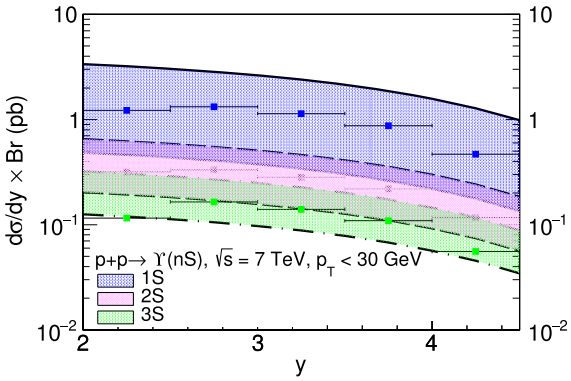

FIG. 10. The rapidity dependence of prompt $\Upsilon(1S)$ (blue solid), $\Upsilon(2S)$ (magenta dashed), and $\Upsilon(3S)$ (green dot-dashed) production at $\sqrt{s} = 7$ TeV integrated over $p_T < 30$ GeV in the ICEM with combined mass and renormalization scale uncertainties are compared with the LHCb data [27].

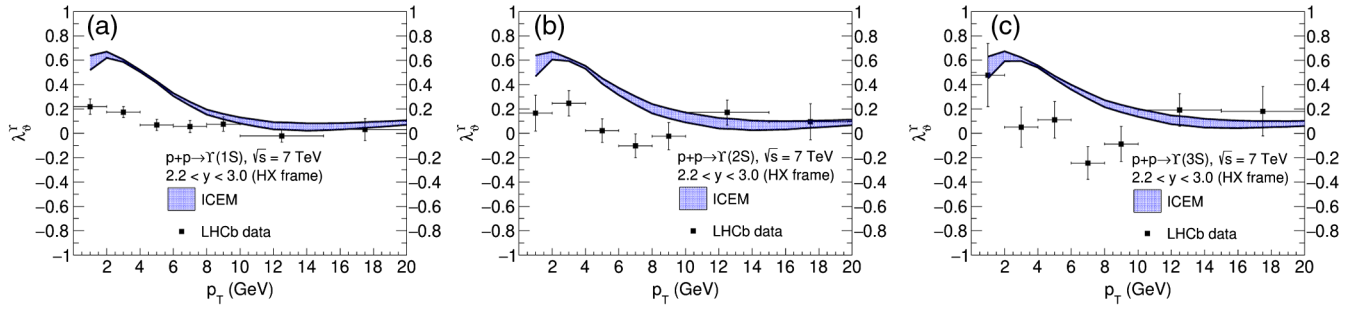

FIG. 11. The p_T dependence of the polarization parameter λ_ϑ for prompt $\Upsilon(1S)$ (a), $\Upsilon(2S)$ (b), and $\Upsilon(3S)$ (c) production in the helicity frame at $\sqrt{s} = 7$ TeV in the ICEM using the "low p_T" c_Q's with mass uncertainties are compared to the LHCb data in the range $2.2 < y < 3$ [31].

We note that the J_z components of the polarized cross section depend differently on the bottom quark mass. When $p_T \leq M_Q$, the longitudinally polarized partonic cross section decreases faster with increasing m_b than the transversely polarized partonic cross section in the helicity frame. Thus increasing the bottom quark mass results in more transverse polarization. When $p_T > M_Q$, the longitudinally-polarized partonic cross section decreases more slowly with increasing m_b than the transversely-polarized partonic cross section. Thus, increasing the bottom quark mass results in more longitudinal polarization. As $p_T \gg \hat{s}, \lambda_\vartheta$ becomes insensitive to m_b. Thus the uncertainty in λ_θ is narrower at high p_T.

Our calculation also depends on the feed-down ratios presented in Table. II, taken from Ref. [13]. Here, "low p_T" refers to $p_T \lesssim 20$ GeV and "high p_T" refers to $p_T \gtrsim 20$ GeV. We use the "low p_T" ratios to compare our results with LHCb data ($0 < p_T < 20$ GeV) and the "high p_T" ratios to compare with the CMS data ($10 < p_T < 50$ GeV).

1. Prompt $\Upsilon(nS)$ polarization in $p+p(\bar{p})$ collisions at low p_T

We present the polarization parameters for prompt $\Upsilon(1S)$ in $p+p$ collisions at $\sqrt{s} = 7$ TeV at forward rapidity ($2.2 < y < 3$) in the helicity frame (HX) in Fig. 11. We compare our results with data from the LHCb Collaboration in the forward rapidity region [31]. The ICEM polarization of prompt $\Upsilon(nS)$ in the helicity frame is slightly transverse at low p_T ($p_T < M_\Upsilon$). The result becomes unpolarized for $p_T > M_\Upsilon$. We do not find that the polarization has any significant rapidity dependence. The ICEM polarization agrees with the LHCb data for $p_T > M_\Upsilon$.

We also compare the polarization parameter for prompt $\Upsilon(1S)$ in $p+\bar{p}$ at $\sqrt{s} = 1.8$ TeV with the data measured by the D0 Collaboration in the region $|y| < 0.4$ [32] in the helicity frame, shown in Fig. 12. We also do not find a strong dependence on $\sqrt{s}$ for the prompt $\Upsilon(1S)$ polarization in the ICEM. The trend in the p_T dependence of the polarization is the same. At the highest p_T bin, the prompt $\Upsilon(1S)$ polarization measured by the D0 Collaboration is slightly longitudinal while still agreeing with the ICEM calculation, which gives an unpolarized result.

We do not find significant differences in the polarizations among the $\Upsilon(nS)$ states. This is because the calculations of the $\Upsilon(nS)$ states differ from one another only by the integration limits of the ICEM. Furthermore, the polarization depends only on the ratio of polarized to unpolarized cross sections. Thus there is only a slight difference in polarization whether only direct production is included or if feed down also contributes. Therefore the polarization of $\Upsilon(nS)$ from χ_b feed down is similar to that for direct production $\Upsilon(nS)$ alone. Thus, varying the feed-down ratio, either by adopting the "high p_T" ratios from Ref. [13] used here or the p_T-independent ratios calculated in Ref. [33] and used in Ref. [3], changes the polarization by less than 0.05 over all p_T. Our results differ from an NLO NRQCD calculation finding that all $\Upsilon(nS)$ states are unpolarized: $(-0.2 < \lambda_\vartheta < 0.2)$ at low p_T [7]. In their approach, at low p_T, the direct $\Upsilon(nS)$ states are slightly longitudinally polarized while the contribution from χ_b feed down is slightly transverse, resulting in unpolarized prompt production.

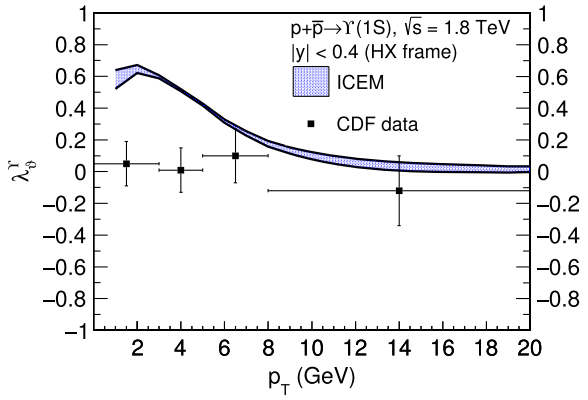

FIG. 12. The p_T dependence of the polarization parameter λ_ϑ for prompt $\Upsilon(1S)$ production in the helicity frame at $\sqrt{s} = 1.8$ TeV with $|y| < 0.4$ in the ICEM using the "low p_T" c_Q's [13] with mass uncertainties are compared to the CDF data [32].

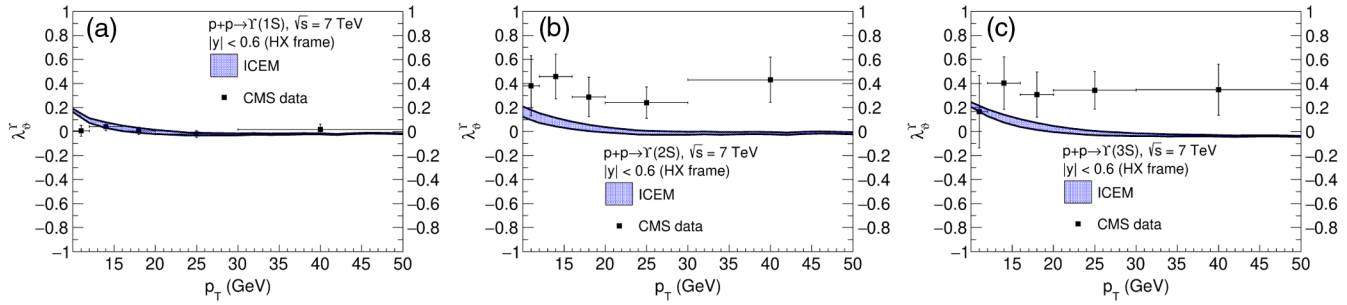

FIG. 13. The p_T dependence of the polarization parameter λ_ϑ for prompt $\Upsilon(1S)$ (a), $\Upsilon(2S)$ (b), and $\Upsilon(3S)$ (c) production in the helicity frame at $\sqrt{s} = 7$ TeV in the ICEM using the "high p_T" $c_\mathcal{Q}$'s [13] with mass uncertainties are compared to the CMS data at midrapidity in the range $|y| < 0.6$ [34].

2. Prompt $\Upsilon(nS)$ polarization in $p+p(\bar{p})$ collisions at high p_T

We present the polarization parameters for prompt $\Upsilon(1S)$ in $p+p$ collisions at $\sqrt{s} = 7$ TeV at central rapidity ($|y| < 0.6$) in the helicity frame respectively in Fig. 13. We compare our results with the data from the CMS Collaboration in the central rapidity region [34]. The ICEM polarization of prompt Υ in the helicity frame is near unpolarized at intermediate p_T ($p_T \sim M_\Upsilon$). We see that λ_ϑ becomes unpolarized for $p_T > M_\Upsilon$. The ICEM polarization agrees with the CMS data for $\Upsilon(1S)$ and only agrees with $\Upsilon(2S)$ and $\Upsilon(3S)$ data within 2σ. We do not find that the polarization has any significant rapidity dependence.

We note that here we have used the "high p_T" set of feed-down ratios to consider the prompt $\Upsilon(nS)$ polarization. Although the contribution from direct $\Upsilon(1S)$ to prompt $\Upsilon(1S)$ drops from 71% to 45%, the polarization of the prompt production does not change significantly. This is because the polarization of all the bottomonium states below the $B\bar{B}$ threshold are very similar after feed down to prompt $\Upsilon(nS)$. We note that the polarization at intermediate p_T, $p_T \sim 15$ GeV, has no significant dependence on the choice of feed-down ratios, as shown in Figs. 11 and 13. The variation of the feed down fractions is negligible compared to the bottom quark mass variation.

Similar to our results at low p_T, we do not find significant differences in polarizations among the $\Upsilon(nS)$ states. Our results differ from an NLO NRQCD calculation finding that the polarization at $p_T \gtrsim 20$ GeV is more transverse for higher mass bound states, saturating at $\lambda_\vartheta \sim 0.2$, ~ 0.4 and ~ 0.9, for $\Upsilon(1S)$, $\Upsilon(2S)$, and $\Upsilon(3S)$ respectively [7]. The significant transverse polarization of $\Upsilon(3S)$ in their approach is due to the fact that the polarization is calculated without the contribution from χ_b feed-down production. In a subsequent update of Ref. [7], where $\chi_b(nP)$ feed-down production is considered, the polarization parameters saturate at $\lambda_\vartheta \sim 0.4$, ~ 0.6, and ~ 0.6 for $\Upsilon(1S)$, $\Upsilon(2S)$, and $\Upsilon(3S)$ respectively [35]. (See also Ref. [36]).

C. Frame dependence of λ_ϑ

We now turn to the frame dependence of our 7 TeV results. We calculate the polarization parameter in $p+p$ collisions at $\sqrt{s} = 7$ TeV in the same kinematic region as presented in Fig. 11 in both the Collins-Soper and the Gottfried-Jackson frames, shown in Figs. 14 and 15

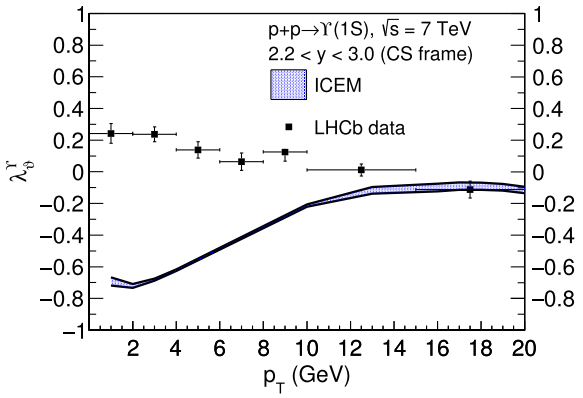

FIG. 14. The p_T dependence of the polarization parameter λ_ϑ for prompt $\Upsilon(1S)$ production in the Collins-Soper frame at $\sqrt{s} = 7$ TeV and $2.2 < y < 3$ in the ICEM using the "low p_T" $c_\mathcal{Q}$'s [13] with mass uncertainties are compared to the LHCb data [31].

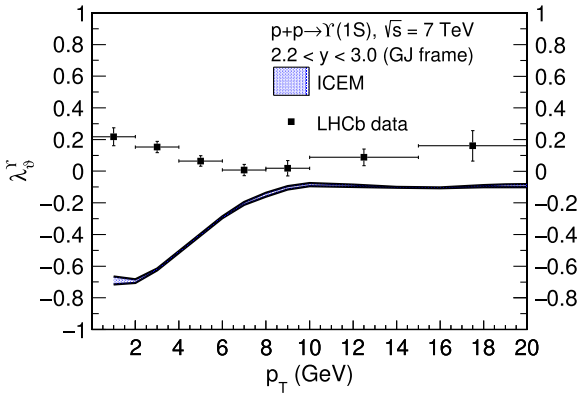

FIG. 15. The p_T dependence of the polarization parameter λ_ϑ for prompt $\Upsilon(1S)$ production in the Gottfried-Jackson frame at $\sqrt{s} = 7$ TeV and $2.2 < y < 3$ in the ICEM using the "low p_T" $c_\mathcal{Q}$'s [13] with mass uncertainties are compared to the LHCb data [31].

respectively. Since the polarization axes in the helicity frame and the Collins-Soper frame are always perpendicular to each other in $\mathcal{O}(\alpha_s^2)$ kinematics, the polarization in the Collins-Soper frame is opposite to that in the helicity frame in the ICEM. Therefore, at low p_T, where the $\Upsilon(1S)$ is predicted to be slightly transverse in the helicity frame, it is predicted to be slightly longitudinal in the Collins-Soper frame. For $p_T > M_\Upsilon$, λ_ϑ is predicted to be unpolarized in both frames. We only find agreement with the data in the Collins-Soper frame for the highest p_T bin. When $p_T \ll m_T$, the angle between the polarization axes in the Gottfried-Jackson frame and that in the Collins-Soper frame is small. As p_T increases, the polarization axis in the Gottfried-Jackson frame becomes collinear with that in the helicity frame. Therefore, the polarization calculated in the Gottfried-Jackson frame is opposite to that in the helicity frame at low p_T and thus similar to that in the Collins-Soper frame. However, as p_T increases, the polarization in the Gottfried-Jackson frame should asymptotically approach the polarization in the helicity frame. Since λ_ϑ is unpolarized in the helicity frame in the high p_T limit, the ICEM polarization becomes frame independent in this limit. We find the ICEM polarization agrees with the data in all frames at high p_T but does not agree with the low p_T data where the frame dependence is most significant.

V. CONCLUSIONS

We have presented the transverse momentum distributions of the prompt $\Upsilon(n\mathrm{S})$ cross section as well as the polarization of prompt $\Upsilon(n\mathrm{S})$ production in $p+p$ and $p+\bar{p}$ collisions in the improved color evaporation model in the k_T-factorization approach. We compared the p_T dependence to data at collider energies. We also presented the ratio $\chi_{b2}(1\mathrm{P})/\chi_{b1}(1\mathrm{P})$ as a function of p_T at $\sqrt{s} = 8$ TeV. We find prompt $\Upsilon(n\mathrm{S})$ production to be unpolarized at $p_T \gtrsim M_\Upsilon$, independent of frame. We do not observe any rapidity or energy dependence in the polarization in the ranges considered.

Since our calculation of the matrix elements is leading order in α_s, we expect improvements when we calculate the cross section to $\mathcal{O}(\alpha_s^3)$ in a future publication.

ACKNOWLEDGMENTS

We thank B. Kniehl for the initiation of and encouragement throughout this project. This work was performed under the auspices of the U.S. Department of Energy by Lawrence Livermore National Laboratory under Contract No. DE-AC52-07NA27344 and supported by the U.S. Department of Energy, Office of Science, Office of Nuclear Physics (Nuclear Theory) under Contract No. DE-SC-0004014.

[1] V. Cheung and R. Vogt, Phys. Rev. D **98**, 114029 (2018).
[2] Y. Q. Ma and R. Vogt, Phys. Rev. D **94**, 114029 (2016).
[3] V. Cheung and R. Vogt, Phys. Rev. D **96**, 054014 (2017).
[4] V. Cheung and R. Vogt, Phys. Rev. D **95**, 074021 (2017).
[5] W. E. Caswell and G. P. Lepage, Phys. Lett. **167B**, 437 (1986).
[6] B. Gong, L. P. Wan, J. X. Wang, and H. F. Zhang, Phys. Rev. Lett. **110**, 042002 (2013).
[7] B. Gong, L. P. Wan, J. X. Wang, and H. F. Zhang, Phys. Rev. Lett. **112**, 032001 (2014).
[8] G. T. Bodwin, E. Braaten, and J. Lee, Phys. Rev. D **72**, 014004 (2005).
[9] J. C. Collins and R. K. Ellis, Nucl. Phys. **B360**, 3 (1991).
[10] B. A. Kniehl, D. V. Vasin, and V. A. Saleev, Phys. Rev. D **73**, 074022 (2006).
[11] V. D. Barger, W. Y. Keung, and R. J. Phillips, Phys. Lett. **91B**, 253 (1980).
[12] F. Hautmann and H. Jung, Nucl. Phys. **B883**, 1 (2014).
[13] A. Andronic *et al.*, Eur. Phys. J. C **76**, 107 (2016).
[14] G. Aad *et al.* (ATLAS Collaboration), Phys. Rev. D **87**, 052004 (2013).
[15] B. B. Abelev *et al.* (ALICE Collaboration), Eur. Phys. J. C **74**, 2974 (2014).
[16] R. Aaij *et al.* (LHCb Collaboration), Eur. Phys. J. C **74**, 3092 (2014).
[17] G. Aad *et al.* (ATLAS Collaboration), Phys. Lett. B **705**, 9 (2011).
[18] V. Khachatryan *et al.* (CMS Collaboration), Phys. Rev. D **83**, 112004 (2011).
[19] R. Aaij *et al.* (LHCb Collaboration), J. High Energy Phys. 06 (2013) 064.
[20] R. Aaij *et al.* (LHCb Collaboration), J. High Energy Phys. 11 (2012) 031.
[21] R. Aaij *et al.* (LHCb Collaboration), Eur. Phys. J. C **72**, 2025 (2012).
[22] S. Chatrchyan *et al.* (CMS Collaboration), Phys. Lett. B **727**, 101 (2013).
[23] P. Faccioli, C. Lourenço, J. Seixas, and H. K. Wöhri, Eur. Phys. J. C **69**, 657 (2010).
[24] G. A. Schuler and R. Vogt, Phys. Lett. B **387**, 181 (1996).
[25] J. C. Collins and D. E. Soper, Phys. Rev. D **16**, 2219 (1977).
[26] K. Gottfried and J. D. Jackson, Nuovo Cimento **33**, 309 (1964).
[27] R. Aaij *et al.* (LHCb Collaboration), J. High Energy Phys. 11 (2015) 103.
[28] S. Abachi *et al.* (D0 Collaboration), DOI: 10.2172/102428.
[29] V. Khachatryan *et al.* (CMS Collaboration), Phys. Lett. B **743**, 383 (2015).
[30] R. Aaij *et al.* (LHCb Collaboration), J. High Energy Phys. 10 (2014) 088.

[31] R. Aaij *et al.* (LHCb Collaboration), J. High Energy Phys. 12 (2017) 110.
[32] D. Acosta *et al.* (CDF Collaboration), Phys. Rev. Lett. **88**, 161802 (2002).
[33] S. Digal, P. Petreczky, and H. Satz, Phys. Rev. D **64**, 094015 (2001).
[34] S. Chatrchyan *et al.* (CMS Collaboration), Phys. Rev. Lett. **110**, 081802 (2013).
[35] Y. Feng, B. Gong, L. P. Wan, and J. X. Wang, Chin. Phys. C **39**, 123102 (2015).
[36] H. Han, Y. Q. Ma, C. Meng, H. S. Shao, Y. J. Zhang, and K. T. Chao, Phys. Rev. D **94**, 014028 (2016).